Infiltration and instability in dune erosion

Margaret L. Palmsten[1,2] and Robert A. Holman[1]

Received 2 March 2011; revised 17 June 2011; accepted 5 August 2011; published 26 October 2011.

[1] Forecasting dune erosion prior to a storm or over longer periods requires knowledge of the fluid forces on the dune sediments. To improve our predictive capability for this process, we propose a new model in which dune slumping occurs when water, which infiltrates horizontally into the dune, increases the overburden sufficiently to destabilize the dune. Horizontal infiltration is driven by suction of water from swash into the dune via capillary action and is a surprisingly strong process with rapid time scales. Because the elevated pore water concentrations increase the apparent cohesion of the wetted sediments, we also propose that the entire volume of wetted sand slumps as a unit when the dune becomes unstable and erosion can be modeled based on the force balance on a sliding block. Several versions of this model were tested, including a numerical infiltration model, a simplified infiltration equation, and an equation based on offshore wave forcing, rather than known forcing at the dune. The model was tested using data from a large-scale laboratory experiment with a storm hydrograph to investigate the time dependence of dune erosion. Predicting slope stability using a numerical infiltration model with known forcing explained 72% of the observed variance in erosion rate, while a simplified stability and infiltration model explained 58%. Error statistics suggest that we captured the majority of the physics controlling dune erosion in this laboratory experiment and that the simplified model will be useful as a forecasting tool.

Citation: Palmsten, M. L., and R. A. Holman (2011), Infiltration and instability in dune erosion, *J. Geophys. Res.*, *116*, C10030, doi:10.1029/2011JC007083.

1. Introduction

[2] Coastal sand dunes provide natural protection for landward lying assets including buildings, infrastructure, and ecosystems. When the combined heights of tide, surge, wave setup, and wave runup during extreme storms exceed the base of the dune, the system is vulnerable to erosion and landward lying assets are at risk. A predictive capability for modeling the vulnerability of dunes to extreme conditions would improve the quality of risk assessments and mitigation in threatened areas. Probabilistic dune erosion forecasts of this type have application on both the short time scale of a storm event and the long-term time scale associated with the cumulative effects of storms and sea level rise. In both cases, simple models are needed for forecasting.

[3] The primary measure of the vulnerability of a dune is the potential volume of sediment that may be eroded during a storm. Typically, these erosion rates are modeled based on one of two time-dependent approaches. In the first, including the models EDune, SBeach, and XBeach [*Kriebel and Dean*, 1985; *Larson and Kraus*, 1989; *Roelvink et al.*, 2009], dune erosion is dependent on a user-defined threshold. Changes in the subaqueous profile are based on cross-shore sediment transport models up to the shallowest location where hydrodynamics may be modeled with a prescribed extrapolation from there to the shoreline or avalanching if the beach profile exceeds a user slope. Each model of this type contains a different set of assumptions for which hydrodynamic process are important [*Kriebel and Dean*, 1985; *Roelvink et al.*, 2009; *van Rijn*, 2009], but all invoke an arbitrary mechanism for the actual dune erosion.

[4] The second type of time-dependent dune erosion model is known as the wave impact model [*Fisher et al.*, 1986; *Overton and Fisher*, 1988; *Overton et al.*, 1994a]. This model hypothesizes that the volume of sediment eroded, ΔV, is proportional to the force of wave impact, F:

$$\Delta V = C_F \sum F, \tag{1}$$

where C_F is a calibration coefficient with units of meter seconds squared per kilogram. F is the force of the bore at impact ($F = \rho u^2 h$), where ρ is the water density, u is the velocity of the bore just prior to impact, and h is the height above the dune base of the wave just prior to impact. *Overton et al.* [1994b] found that C_F depended on grain size and compaction.

[5] The wave impact model provided a basis for the dune erosion model of *Larson et al.* [2004]. In this model, ΔV is parameterized in terms of the height of wave runup, R, above the dune base, z_b, and the time R exceeded z_b, Δt_R:

$$\Delta V = 4C_L(R - z_b)^2 \frac{\Delta t_R}{T}, \tag{2}$$

[1]College of Oceanic and Atmospheric Sciences, Oregon State University Corvallis, Oregon, USA.
[2]Now at Naval Research Laboratory, Stennis Space Center, Mississippi, USA.

0148-0227/11/2011JC007083

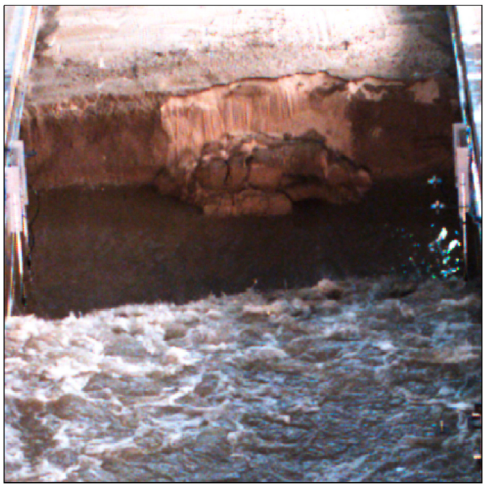

Figure 1. Image of the dune just after a slump occurred. The wet slumped material is visible on the foreshore, along with the dry material on the dune scarp.

where C_L is a nondimensional calibration coefficient dependent on grain size and wave height and T is the incident wave period. *Palmsten and Holman* [2011], tested equation (2) using detailed observations of runup and dune erosion from a large wave flume experiment. They found that equation (2) explained 64% of the observed erosion volume.

[6] Although the wave impact model has the advantage of directly addressing the interaction between waves and sediments of the dune face, the assumption that the volume of eroded sediment is dependent on the normal force impacting the dune face is not obvious, since slumping is caused by the balance of forces acting along failure planes within the dune and not on normal forces.

[7] *Erikson et al.* [2007] investigated the instability of undercut dunes that lead to slumping in their laboratory investigation of dune erosion. The size of the overhang was determined using an approach similar to equation (2). The presence of the overhang caused a bending moment and tension crack that were modeled using elastic beam theory [*Erikson et al.*, 2007]. Using this approach, they were able to accurately model scarp recession distance (R^2 between model and observation was 0.90). However, their theory and observations were limited to the case of overhanging dunes, and no erosion would occur in the absence of undercutting.

[8] In a recent dune erosion experiment [*Palmsten and Holman*, 2011] we made three observations that inform the hypotheses for a new dune erosion model. First, we observed that dune slumping occurred only after water had infiltrated the dune for some time. Second, we observed that the slump usually involved only the wet portion of the dune sediments, leaving the scarp surface dry (Figure 1). Finally, we observed that the dune reached a stable state when the dune base eroded upward, so scarp height became smaller than some critical scarp heights. These observations suggest the hypothesis that the primary cause of dune erosion in the experiment is slope instability caused by the excess overburden associated with the weight of infiltrated pore water.

[9] The overall objective of this work is to develop a simple model for dune erosion that accounts for the effect of infiltration that is due to the time-dependent exposure of dune sediments to waves. In the proposed dune erosion model, we invoke slope instability as the driving mechanism for dune slumping and infiltration of water into the dune as the dominant control on strength of the sediment and excess weight. We hypothesize that the dune erodes when the destabilizing force along the failure plane exceeds the resisting strength of the sediment. Furthermore, on the basis of our observation that the wetted dune tended to slump, we hypothesize that the volume of material eroded from the dune is equivalent to the volume of material that has been infiltrated by waves; thus, the eroded volume will be equal to the infiltrated volume, a simple principle for practical estimation.

[10] In the next section of this paper, we describe the equations for infiltration of water into the dune and slope stability. In sections 3 and 4, we describe the experimental methods used in the wave flume experiment and the results of the experiment compared with different versions of the proposed dune erosion model. Finally, in sections 5 and 6, we discuss results and make conclusions.

2. Dune Erosion Model

[11] We propose that dune slumping occurs when water, which infiltrates horizontally into the dune, increases the overburden sufficiently and destabilizes the potential sliding mass. Horizontal infiltration is driven by the capillary action of water wicking into the dune. The elevated pore water content caused by infiltration also increases the apparent cohesion of the wetted sediments. As a result, the wetted volume of sand slumps as a single unit and is modeled as the force balance on a sliding block.

2.1. Infiltration Model

[12] In order to model infiltration of water into the dune, we use Darcy's law for the flux of water q (in units of meters cubed per second per square meter of surface), through porous media:

$$q = -K(\psi)\frac{\partial \psi}{\partial x}, \tag{3}$$

where K is the hydraulic conductivity in units of meters per second, ψ is the pressure head in units of meters of water, and x is the cross-shore axis. Both K and ψ are dependent on the volumetric water content of the pore spaces, θ, in units of meters cubed per meters cubed. The relationship between these variables is given later in this section.

[13] The flux of water into a relatively dry dune is driven by a process called matric suction. Matric suction is caused by the capillary force (twice the ratio between surface tension of the water and radius of curvature of the meniscus) when both water and air occupy the space between sand grains. In partially saturated sediment, the surface tension causes a compressive force on the sand grains, acting to hold the grains tightly together [*McCarthy*, 2007]. As the amount of air in the pore space decreases, the radius of curvature of the meniscus increases, and as a result the matric suction decreases. By convention, pore water pressure head, ψ, under matric suction is negative, so that the gradient in pressure between water from swash and unsaturated sediments drives flow into the dune.

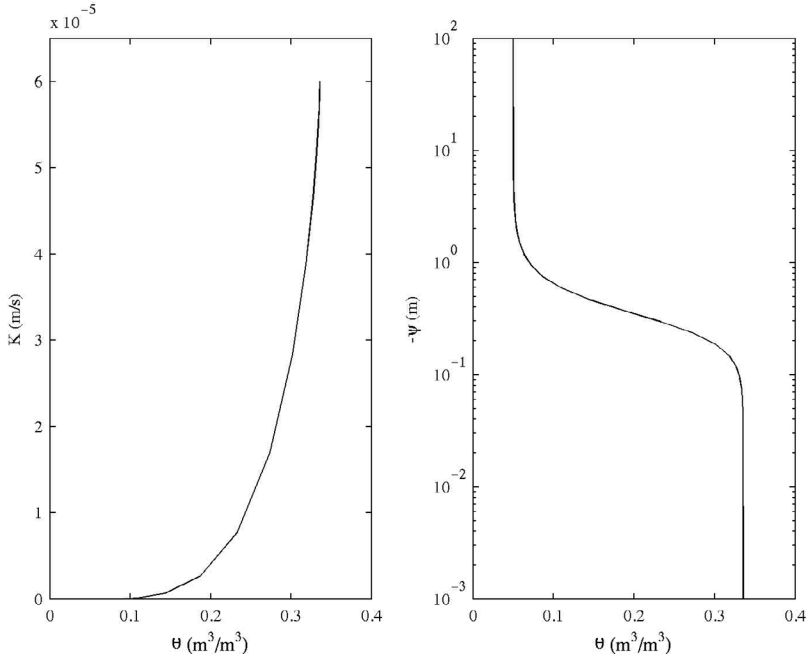

Figure 2. Plots of equation (5) and (6) using the hydraulic properties of the *Schaap and Leij* [2000] PTF.

[14] Another possible force contributing to the infiltration of water into the dune is the force of wave impact, F, in equation (1). F was estimated using video observations of bore velocity, u, and height of runup at impact, h. The pressure gradient between wet and dry sand was estimated to be approximately an order of magnitude larger than typical values for F. Therefore, matric suction was the only force assumed to be driving water into the dune.

[15] Equation (3) is substituted into the continuity equation to determine infiltration of water into the dune [*Richards*, 1931] as

$$\frac{\partial \theta}{\partial t} = \frac{\partial}{\partial x} K(\psi) \frac{\partial \psi}{\partial x}. \tag{4}$$

[16] K describes the relative ease with which water flows through sediment. Both K and ψ are functions of θ, so they can also be expressed as functions of each other. *van Genuchten* [1980] derived an analytical expression for K:

$$K(\psi) = \frac{1 - (\nu\psi)^{n-2}[1 + (\nu\psi)^n]^{-m}}{[1 + (\nu\psi)^n]^{2m}}, \tag{5}$$

where ν and n are parameters that must be estimated from sediment data and $m = 1 - 1/n$. ψ is related to θ [*van Genuchten*, 1980] as

$$\theta = \theta_r + \frac{(\theta_s - \theta_r)}{[1 + (\nu\psi)^n]^m}, \tag{6}$$

where θ_r is residual water content and θ_s is saturated water content.

[17] When hydraulic properties are not directly measured, the values of the hydraulic properties θ_r, θ_s, ν, n, and $K(\psi)$ for a particular sediment type may be determined using a pedotransfer function (PTF) that relates hydraulic properties to sediment characteristics, including percentage of sand, silt, and clay, median grain size, bulk density, or percentage of organic content. The choice of PTF is important because it ultimately determines the rate of infiltration into the dune.

[18] PTFs are typically developed using regression or neural network analyses on data sets in which both the sediment and hydraulic properties are known. PTFs depend strongly on the data set from which they are developed. Ideally, a PTF developed from a large database with a variety of sediment types, or one with similar sediment characteristics to the sediment of interest, should be used [*Wösten et al.*, 2001]. We selected the PTF developed by *Schaap and Leij* [2000] since 43% of the samples from the calibration data set were classified as sand. Plots of equations (5) and (6) using sediment characteristics and the *Schaap and Leij* [2000] PTF are shown in Figure 2.

[19] Given sediment and hydraulic properties, equation (4) may be solved numerically using a model, for example Hydrus1D [*Šimůnek et al.*, 2005], and the following boundary conditions. The pressure head at the surface of the dune is taken to be 0 m ($\psi = 0$ m at $x = x_b$ m, the cross-shore location of the dune scarp) when swash is in contact with the dune since there is no hydrostatic pressure below a swash surface falling in ballistic motion, and the force of wave impact on the dune face is assumed to be small relative to the pore water pressure gradient. When waves recede from the dune face, the boundary condition is altered to require that the flux of water into the dune be 0 m^3 (m^2)$^{-1}$ s^{-1} ($q = K(\psi)\frac{\partial \psi}{\partial x} = 0$ m^3 (m^2)$^{-1}$ s^{-1} at $x = x_b$). The boundary condition at the interior boundary of the solution domain, away from infiltration, is also taken to be a no-flux condition. The dune is initially assumed to have $\theta = \theta_r$. The dune face boundary conditions were alternated as a function of the presence or absence of swash on the dune scarp based on the measured swash time series from the

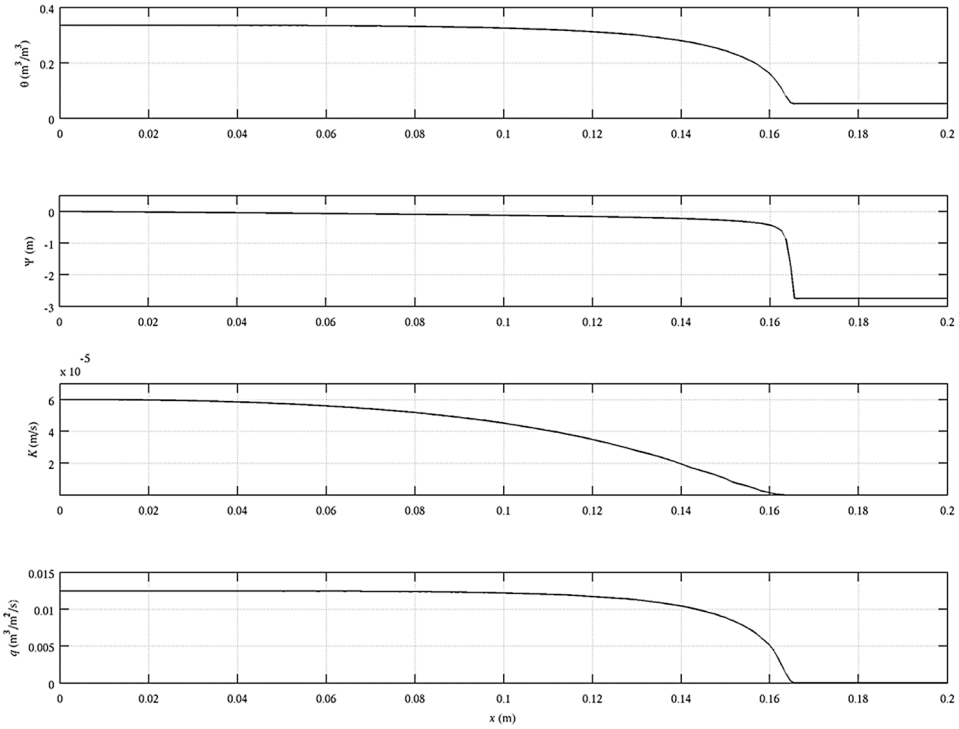

Figure 3. An example of Hydrus 1D model results after the dune was exposed to swash.

experiment. θ, ψ, K, and q are plotted as functions of x in Figure 3 to demonstrate a typical solution to equation (4) after the dune is exposed to 15 min of swash.

2.2. Simple Infiltration Model

[20] The most accurate solution comes from solving equation (4) numerically using a measured swash time series. However, this full solution is both complicated to execute and impossible to use in a predictive sense when time series data are unavailable. As a practical solution, we also explore a simplified representation of infiltration. In this representation, the dune face boundary is assumed to be constantly wetted ($\psi = 0$ m) for the integrated time that the dune is exposed to swash; then it is assumed to be dry (no flux) for the remainder of each 15 min analysis period representing the integrated time that the dune face is exposed to air.

[21] This approach has two advantages. First, infiltration may be modeled using the full solution to equation (4) when the time series of swash on a dune is unknown, but an estimate of exposure time from offshore wave conditions is known. Second, a significantly more simple equation for infiltration into the dune may be implemented for the case of constant exposure, one that does not require a numerical model to solve.

[22] *Green and Ampt* [1911] derived this simplified approach by assuming that the water infiltrated into the dune can be approximated by a region of constant water content, $\Delta\theta$, that has infiltrated a distance, Δx_I. The flux of infiltrated water, q, is related to the change in position of the wetted front as

$$q = \Delta\theta \frac{\partial x}{\partial t}. \tag{7}$$

[23] *Green and Ampt* [1911] assumed that the pore spaces in soil could be modeled as capillary tubes under steady flow conditions. Thus, the pressure gradient in Darcy's law (equation (3)) can be represented by the bulk gradient, $\Delta\psi/\Delta x_I$. Combining Darcy's law and equation (7), we can represent Δx_I as a function of period of exposure, Δt:

$$\Delta x_I(t) = \left(\frac{2K\Delta\psi\Delta t}{\Delta\theta}\right)^{1/2}. \tag{8}$$

[24] *Green and Ampt* [1911] showed that the wetted region is not entirely saturated for horizontal infiltration, so $\Delta\theta$ was set to 0.70, based on the average value of $\Delta\theta$ from the solution of the Richards equation (equation (4)). Values for K and $\Delta\psi$ were determined using the same PTF as in the full model, but assuming full saturation, since the driving pressure head is the difference between the swash and the dry dune sand.

[25] The application of equation (8) is strictly for the cumulative time for which the dune was exposed to swash and underestimates infiltration, since the infiltration that occurs between swashes is neglected. We account for these differences in infiltration distance that are due to swash intermittency by multiplying Δx_I from equation (8) with an empirical constant:

$$\Delta x_\Lambda = \Lambda \Delta x_I. \tag{9}$$

[26] The value for Λ was calibrated using data collected between hours 10 and 10.25 of the dune erosion experiment. Results of the calibration are described in section 4.3.

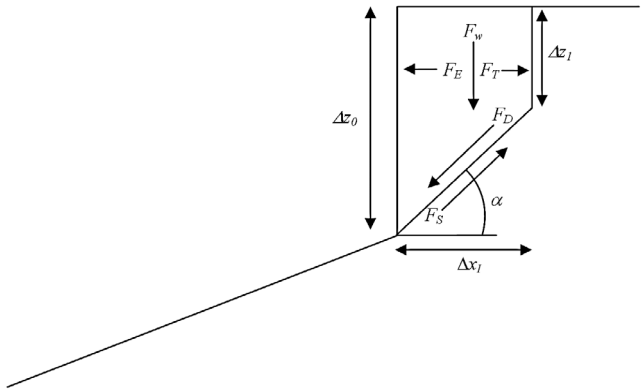

Figure 4. Schematic drawing of dune failure including vertical cleavage.

2.3. Wave Runup Model

[27] Ideally, the observed continuous time series of the swash edge on the dune would be used as boundary conditions for the infiltration model. However, in most cases direct observations of swash edge are unavailable and only offshore wave data are available. One solution would be to run a time-dependent model over the known nearshore bathymetry to determine a full time series of the swash edge. However, the bathymetry data required for executing this approach are rarely available. This approach would also add significant computational effort to the model.

[28] An alternative, simpler approach is to use empirical relationships for the surf zone transformation processes to predict the statistics of runup based only on offshore wave conditions and a bulk measure of beach slope. Wave runup, R, is defined as the maximum vertical excursion of the swash time series above the still water line. *Stockdon et al.* [2006] developed an equation relating the elevation of the highest 2% of wave runup, R_2, to offshore wave conditions based on video observations from 10 field experiments covering a range of beach types and wave conditions. The equation is based on the assumption of a normal distribution of swash elevations. The runup is composed of a contribution from the mean water level, $\langle\eta\rangle$,

$$\langle\eta\rangle = 0.35\beta(H_0L_0)^{1/2} \tag{10}$$

and a contribution from the standard deviation of swash, σ,

$$\sigma = \frac{[H_0L_0(0.563\beta^2 + 0.0004)]^{1/2}}{4}, \tag{11}$$

where H_0 is the deepwater wave height, L_0 is the deepwater wavelength, and β is the prestorm beach slope determined by regression on the beach profile between the still water line and the dune base. The elevation of the highest 2% of runup is

$$R_2 = 1.1(\langle\eta\rangle + 2\sigma), \tag{12}$$

consistent with the statistics of a normal distribution.

[29] Because equation (12) is based on the normal distribution of the swash time series, it may be reformulated to give the cumulative time that elevation, z, on the dune was exposed to swash, Δt_ε:

$$\Delta t_\varepsilon(z_R + z_{\mathrm{swl}} > z) = [p(z_R + z_{swl} > z)]\Delta t_R, \tag{13}$$

where z_R is the elevation of the swash edge about the still water line, z_{swl} is the elevation of the still water line, p is the cumulative normal distribution defined by $\langle\eta\rangle$ and σ, and Δt_R is the length of time modeled. Δt_ε may be inserted into equation (8) to solve for the depth of infiltration. Although equations (11), (12), and (13) were developed assuming a single beach slope, *Palmsten and Holman* [2011] found them to be reasonable estimators of extreme runup statistics on the dune.

2.4. Dune Stability and Eroded Volume

[30] Once the time-dependent weight of wetted sediment is determined using an infiltration model, the frequency of slumping can be analyzed based on slope stability criteria. Slope stability depends on the magnitude of forces that tend to produce failure and the forces that resist failure along the potential failure plane.

[31] For this analysis, the dune is assumed to be composed of two regions. One region is wetted by infiltration of water from swash, and the region is defined by apparent cohesion values greater than 400 Pa. A second, dry region is defined where apparent cohesion is less than 400 Pa. When fully saturated, the weight of the wetted region is 20% greater than its dry weight because of the addition of water to the pore spaces. Up to the point of near saturation, infiltrated water increases sediment cohesion and the shear strength of the wetted region, and so this region can be assumed to behave as a single unit, a trapezoidal sliding block (Figure 4). Two planes define the sliding block, one plane passing through the base of the dune with a slope, α, determined by interior force balances, and a second failure plane caused by vertical cleavage in the upper portion of the dune. The second plane is located at the boundary between the portion of the dune that has been infiltrated and the portion of the dune that remains at the initial apparent cohesion.

[32] The following analysis develops a number of concepts. In section 2.4.1, the slope of the failure plane with angle, α, is found by examining forces along any plane within the dune. It is shown that failure occurs at a particular plane α, along which the ratio of destabilizing to stabilizing forces is a maximum. In section 2.4.2, the forces on the trapezoidal sliding block are then determined and expressed in terms of destabilizing forces that cause failure because of the increased overburden as the moisture content and volume of the trapezoidal block increase with infiltration and stabilizing forces that resist failure because of the strength of the sediment. The destabilizing forces, F_D, include the downslope components of weight, F_w, and lateral earth force, F_E, acting along the failure plane, while the stabilizing forces, F_S, include forces created by the shear strength of sediments along the bottom failure plane and tensile strength along the vertical plane.

2.4.1. Angle of the Failure Plane

[33] The angle of the failure plane, a, is the least stable angle within the dune. It is the angle at which the difference between the destabilizing shear stress, τ_D, and the critical shear stress is the maximum, and it may be determined by finding the zero derivative of $\tau_D - \tau_{\mathrm{cr}}$ as a function of α.

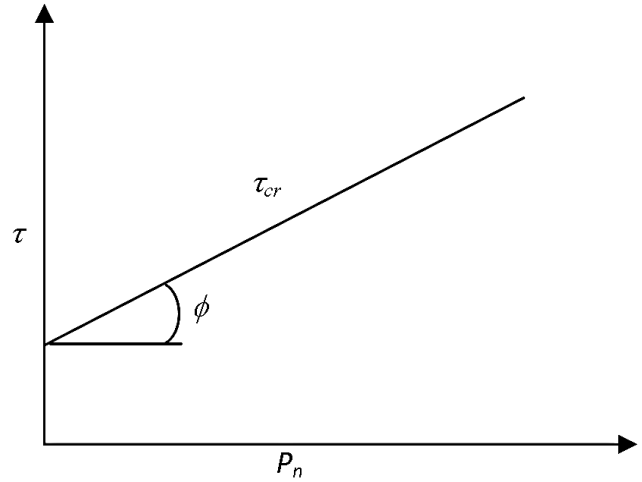

Figure 5. A schematic Mohr stress diagram depicting equation (14). The y intercept represents the contribution of the cohesion and apparent cohesion, the first and third terms in equation (14). The slope of the line depends upon ϕ, a characteristic of the sediment.

[34] The ability of the sediment to resist movement depends on the critical shear strength for unsaturated sediment τ_{cr}:

$$\tau_{cr} = \xi + (P_n - P_a)\tan\varphi + (P_a - P_\omega)\Theta\tan\varphi, \qquad (14)$$

where ξ is cohesion, in units of Pascals per meter alongshore [*Vanapalli et al.*, 1996]. Figure 5 depicts equation (14) in graphical form. P_n the is normal stress on the plane of failure:

$$P_n = \frac{F_w \cos^2\alpha}{\Delta x_I}, \qquad (15)$$

where F_w is the weight the potentially unstable block, in Newtons, that is due to both the weight of the sediment and infiltrated water; α is the angle of the failure plane with respect to the horizontal; Δx_I is the length of the horizontal component of the failure plane, in units of meters, equivalent to the distance water has infiltrated the dune; and $\Delta x_I/\cos\alpha$ is the length of the failure plane. P_a in equation (14) is pore air pressure relative to local atmospheric pressure and is assumed to be 0 Pa. P_ω is the pore water pressure, in Pascals, and is related to the pressure head by $P_\omega = \rho g\psi$. P_ω is a negative value for unsaturated sediment, as discussed in section 2.1, Θ is the relative water content, related to the volumetric water content as $\Theta = \dfrac{\theta - \theta_r}{\theta_s - \theta_r}$, and ϕ is the internal friction angle.

[35] Here τ_{cr} is composed of three terms. The first term accounts for cohesion, the additional strength provided to sediment by electrostatic forces or cementation, which is near 0 Pa for dune sand containing a minimal amount of clay. The second term accounts for the stabilizing frictional force on the shear plane that is due to the reaction to the weight of the overlying sediment.

[36] The final term accounts for the effect of apparent cohesion, sometimes known as the "sandcastle effect," which is due to the presence of unsaturated pore space [*Hornbaker et al.*, 1997]. This term is significant because the additional shear strength gives unsaturated dunes and sandcastles the ability to produce very steep scarps, or overhangs, as water content increases, up to a point where strength begins to decrease (Figure 6). Apparent cohesion is a function of the normalized surface area within the pores over which matric suction acts. *Vanapalli et al.* [1996] found that the normalized area was well predicted by the relative water content Θ.

[37] The second stress needed to determine α is the destabilizing shear stress τ_D, defined as

$$\tau_D = \frac{F_w \sin\alpha\cos\alpha}{\Delta x_I} \qquad (16)$$

in units of Pa/m alongshore. Subtracting τ_D and τ_{cr}, then finding the zero derivative with respect to α yields

$$\alpha = \frac{\pi}{4} + \frac{\varphi}{2}, \qquad (17)$$

relating the failure plane to ϕ, the internal friction angle, a characteristic of the sediment. The failure plane is assumed to pass through the base of the dune. The assumption of α as the angle of the potential failure plane has been shown to accurately quantify the stability of bluffs [*Lohnes and Handy*, 1968] and was also shown to contribute to the failure of overhanging dunes [*Erikson et al.*, 2007].

2.4.2. Force Balance on the Sliding Block

[38] In this subsection, the force balance along the plane defined by α is derived. The balance depends on destabilizing forces, F_D, including the downslope components of weight, F_w, and lateral earth force, F_E, and the stabilizing forces, F_S, including forces created by the shear strength of

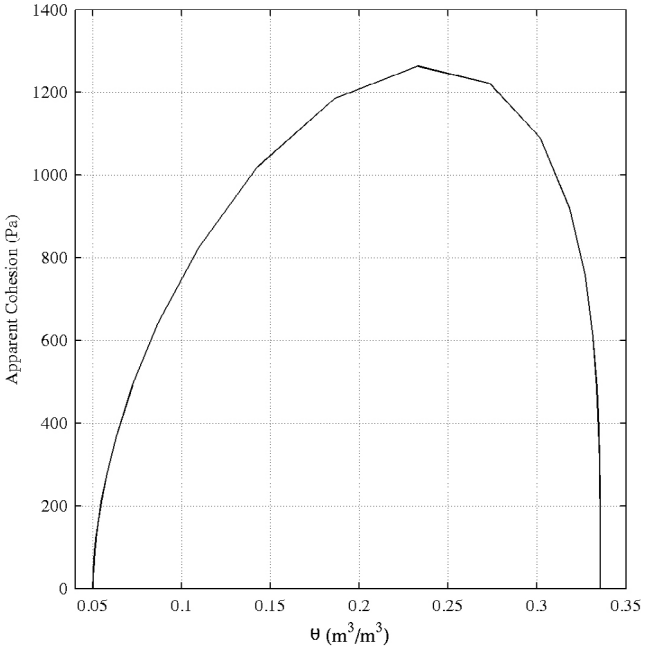

Figure 6. Apparent cohesion as a function of water content for the sand used in this experiment. Shear strength of the sediment increases up to 63% saturation, then begins to decrease.

sediments along the bottom failure plane and tensile strength along the vertical plane.

[39] Unlike that in water, pressure in sediment is anisotropic (weaker in the horizontal than in the vertical) because the sand matrix supports a fraction of its weight. In a vertical scarp, the remaining, unbalanced lateral component of earth force, F_E, is directed outward (Figure 4) and contributes to F_D. In engineering, retaining structures are frequently built to resist the lateral earth force [*McCarthy*, 2007].

[40] The magnitude of the lateral earth force for cohesive soil at the moment when a vertical scarp fails was derived by *Terzaghi and Peck* [1967]. Here, we develop a similar derivation to describe the shear strength of unsaturated sediment, in which both cohesion and the apparent cohesion that is due to the presence of water oppose the lateral earth pressure. To determine lateral earth force, geometry is used to relate shear strength (τ_{cr}) and normal stress (P_n) to the horizontal (P_h) and vertical (P_v) components of stress [*McCarthy*, 2007] when τ_{cr} and τ_D are balanced:

$$\tau_{cr} = \frac{P_h - P_v}{2}\sin 2\alpha, \tag{18}$$

$$P_n = \frac{P_h + P_v}{2} + \frac{P_h - P_v}{2}\cos 2\alpha, \tag{19}$$

Substituting equations (18) and (19) into equation (14) yields

$$P_h = \frac{2\xi}{\tan\alpha} + \frac{P_v}{\tan^2\alpha} + (-P_\omega)\Theta\left(1 - \frac{1}{\tan^2\alpha}\right). \tag{20}$$

[41] The fraction of vertical pressure transferred to the horizontal direction is $\tan^{-2}\alpha$ and is known as the coefficient of earth pressure [*Terzaghi and Peck*, 1967]. P_v at depth $z_c - z$, where z_c is the elevation of the dune crest, depends on pressure of the sediment above, so $P_v = \rho_s g(z_c - z)$, where ρ_s is the bulk density of sediment, and g is gravitational acceleration. Integrating P_h over the dune face and assuming cohesionless sediment yields the lateral earth force:

$$F_E = \frac{\rho_s g \Delta z_0}{2\tan^2\alpha} - (P_\omega)\Theta\left(1 - \frac{1}{\tan^2\alpha}\right)\Delta z_0, \tag{21}$$

where Δz_0 is the height of the dune scarp ($z_c - z_b$).

[42] The effect of the second term allows the direction of F_E to vary based on the magnitude of the apparent cohesion and the height of the dune scarp. When the first term in equation (21) is larger than the second (large Δz_0), F_E is directed out of the dune and contributes to the destabilizing force along the shear plane. However, when the contribution from the apparent cohesion exceeds the lateral earth force (small Δz_0), F_E is directed into the dune and provides a stabilizing force along the shear plane.

[43] *Lohnes and Handy* [1968] derived a force balance for loess bluffs composed of homogeneous, cohesive sediments with tension cracks assuming a trapezoidal sliding block. Here, we take a similar approach, but include apparent cohesion in the derivation, and we assume a tension crack did not exist.

[44] Given the typically steep slopes associated with eroding dunes, dunes may become unstable because of shear failure when the destabilizing force, F_D, exceeds the resisting force associated with shear strength of the sediment, F_S (Figure 4).

[45] F_D is defined as

$$F_D = F_w \sin\alpha + F_E \cos\alpha. \tag{22}$$

For the assumed trapezoidal shape, the weight of the potential slump block is given by

$$F_w = (\rho_s g + \rho g\theta)\left(\Delta z_D - \frac{\Delta x_I \tan\alpha}{2}\right)\Delta x_I. \tag{23}$$

[46] The resisting force on the wetted block, F_S, depends on both the shear strength along the plane, α, and on the tensile strength of the dry sand resisting movement along the vertical plane of weakness, Δz_1. The tensile strength may be determined by substituting apparent cohesion, the third term from equation (14), into the definition for tensile force given by *Lu et al.* [2009], yielding

$$F_T = 2(-P_\omega)\Theta\tan\phi\tan\left(\frac{\pi}{4} - \frac{\phi}{2}\right)\Delta z_1. \tag{24}$$

[47] Finally, combining the stabilizing forces results in the equation for shear strength of the wetted block:

$$F_S = \left(F_W\cos\alpha + F_E\sin\alpha + (-P_\omega)\Theta\frac{\Delta x_I}{\cos\alpha}\right)\tan\phi + F_T. \tag{25}$$

[48] Because the direction of F_E varies based on the magnitude of the apparent cohesion and the height of the dune scarp, its effect on equation (25) also varies. When F_E is directed outward, it acts to reduce the normal force on the failure plane. At times when F_E is directed into the dune, it contributes to the normal force, thus increasing resistance to failure.

[49] When F_D exceeds F_S, we assume that slope instability causes slumping of sediment onto the beach face. From observations, we assume that the wetted sediments slump as an intact block so that the eroded volume is equal to the wetted volume. The latter volume can, in turn, be found as $\Delta V = \sum \Delta x_I\,(z)\Delta z_r$, where Δx_I is the horizontal distance water has infiltrated the dune and Δz_r is the vertical resolution of the modeled dune scarp. Thus, the prediction of dune erosion rates depends only on the estimation of infiltration rates and the determination of time-dependent dune stability.

3. Dune Erosion Experiment

[50] Observations of dune erosion in nature are not readily available because of challenges in acquiring data during storm conditions. Therefore, we conducted a dune erosion experiment in the large wave flume at the Oregon State University Hinsdale Wave Research Lab. The large wave flume is 103 m in length, 3.7 m wide, and 4.6 m deep. The offshore end of the tank was equipped with a flap wave maker, and the onshore end of the tank had a beach made of Oregon beach sand (D_{50} = 0.23 mm). The sediment consisted of 95.50% sand, 2.51% silt, and 1.99% clay, based on grain size analysis of dune sediment, and organic materials comprised <0.01% of the sediment. Bulk density of the

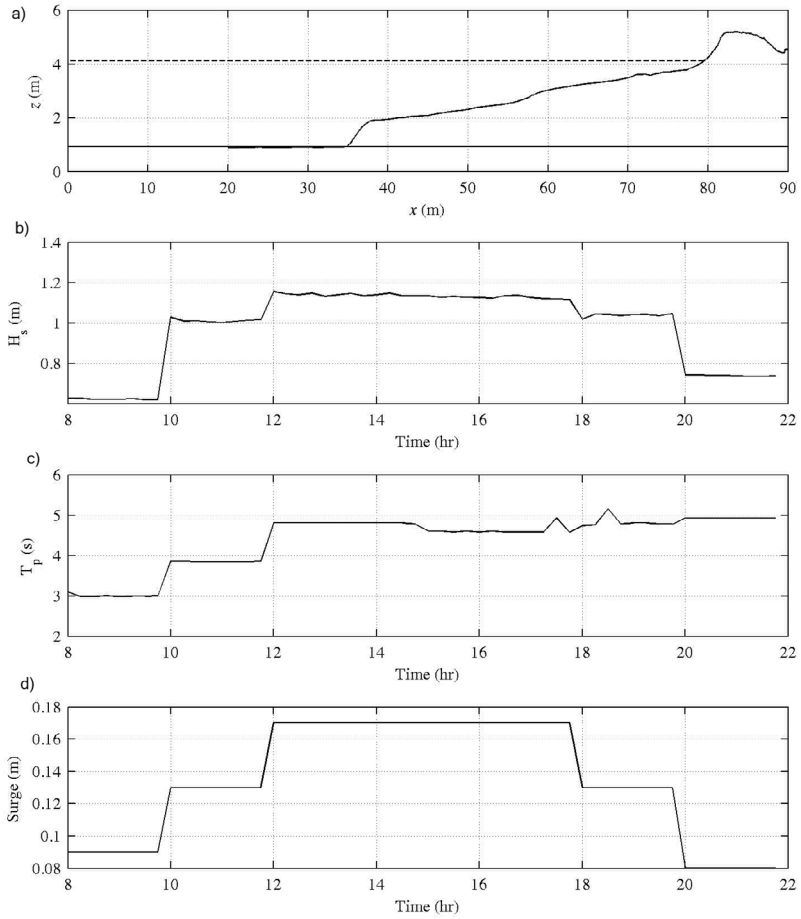

Figure 7. (a) The initial beach profile, (b) wave height at the wave maker, (c) peak wave period, and (d) surge throughout the experiment. The model spatial scaling was 1/6, and the temporal scaling was $1/6^{-0.5}$.

sediment was 1.67 g/cm^3. The initial beach profile consisted of a low sloping subaqueous beach (tan β = 0.04) and a more steeply sloping dune (tan β = 0.5). Wave conditions were designed to be representative of a northeaster storm that occurred near Assateague Island (Maryland-Virginia) in February 1998. Wave height, period, and water level in the tank were adjusted to reflect prototype storm conditions observed at National Buoy Data Center Buoy 44004 off Cape May, New Jersey. Irregular waves were generated by the wave-maker using a TMA spectrum. The time series of wave conditions at the wave maker and the initial beach profile are shown in Figure 7.

[51] Wave forcing on the dune was determined by making observations of the time-varying vertical elevation of the shoreline. The location of the swash edge along the center of the wave flume was determined as a function of time by digitizing the wave-beach intersection from video observations [*Holman and Stanley*, 2007] using a semi-automated routine [*Palmsten and Holman*, 2011]. Then the digitized pixel location of the swash edge was projected onto the beach profile to determine the continuous time series of swash on the beach. The time series of swash elevation was used as input to the Hydrus1D model for horizontal infiltration of water into the dune.

[52] The dune response to wave forcing was determined using stereo video observations of the beach surface every 15 min throughout the experiment (see *Palmsten and Holman* [2011] for a full description of the experimental setup and data quality). Full profiles of the subaerial beach, along with error estimates, were calculated from the video observations. Resolutions of the dune were 0.1 m in the horizontal and 0.04 m in the vertical. Errors in the stereo technique were of the order of 0.02–0.08 m when compared with in situ surveys. The volume of eroded sediment was determined by subtracting consecutive profiles every 15 min and integrating the difference in elevation between the dune base and the dune crest. The resulting erosion rates are reported as meters cubed per meter alongshore per 15 min.

4. Results

[53] Our analysis of the infiltration and slope stability model is divided into three major sections. First, we present experimental observations of dune erosion and wave forcing. Next, we evaluate the infiltration and slope stability model solved using the Richards equation and forced with known conditions by comparing predicted erosion rate with observations. The numerical model tests our understanding of the physical processes causing dune slumping, although we do not measure infiltration. Finally, in order to develop a practical approach to modeling dune erosion, the simplified modeling approach is compared with observed erosion rates

in two steps. This simplified approach is representative of a situation in which dune erosion must be forecast over a large region just prior to passage of a hurricane when only offshore wave forecasts are available. In the simplified approach, erosion is first determined using the combined infiltration and stability model in which infiltration is determined by the modified Green-Ampt equation, equation (9), with known forcing to test the reliability of the equation. Then, the infiltration and stability model is solved with a modified Green-Ampt equation forced with offshore wave conditions and equation (13) to test the efficacy of using the parameterized forcing.

4.1. Observations of Wave Forcing and Dune Erosion

[54] Dune erosion is forced by swash interaction with the dune. Here, we present observations of swash duration on the dune and resulting dune erosion (Figure 8). The beach profiles from stereo observations are plotted in Figure 8a. The fraction of time that the dune was observed to be exposed to swash is shown in Figure 8b. Regions of the beach below the dune base are shown in white. Erosion rate and frequency of slumping events are shown in Figures 8c and 8d.

[55] Combining information from Figure 8, the complex relationship between wave forcing and dune response may be synthesized. Initially, the base of the dune was low on the beach, and swash contacted the dune more than 30% of the time. As the dune base eroded upward between hours 8 and 9, dune exposure to swash decreased. Between hours 9.25 and 10, no slumping was observed.

[56] When wave forcing and water level increased at hour 10, the dune base decreased in elevation, increasing dune exposure to waves. During constant conditions between hours 10 and 12, the elevation of the dune base again increased, limiting dune exposure to swash and resulting in a corresponding decrease in eroded volume of sediment. Slump frequency between hours 10 and 12 was one slump per 15 min period, except at hour 11.25, when two slumps were observed. Slump volume decreased over this 2 h period of constant wave conditions.

[57] Flux from the dune increased after hour 12, when wave height, period, and still water level increased to a maximum. Flux decreased as the dune base eroded upward under continued constant wave conditions between hours 12 and 14. After hour 14, slumping events became more intermittent and eroded volume decreased. Between hours 16 and 18, the elevation of the dune base decreased. At the same time, slumping became more intermittent compared with that earlier in the experiment. Dune slumping ceased after hour 19.5.

4.2. Comparison of Full Model Results and Observed Erosion

[58] In this first comparison between model results and observations, we implement the numerical solution to the Richards equation and force the model with observed conditions at the dune face. The objective of this comparison is to determine our understanding of the physical processes driving dune erosion, both infiltration of swash into the dune and the resulting dune instability.

[59] The basic premise of this dune erosion model is that infiltration of water into the dune adds excess weight, causing it to slump. We first neglected the potentially limiting role of dune stability to focus on the model assumption that the volume of sediment infiltrated by water is proportional to the volume of sediment eroded from the dune. In this approach, the Richards equation, equation (4), was solved using known forcing and beach profiles, and the ratio of destabilizing to stabilizing forces, F_S/F_D, was assumed to be less than 1.

[60] The volume of infiltrated sediment is compared with observations of eroded volume throughout the experiment (Figure 9, top). Simply assuming that the dune was unstable throughout the experiment and the infiltrated volume determined with the Richards equation is proportional to eroded volume reproduced 64% of the observed variance in erosion, suggesting that infiltration is an important component of dune slumping. Bias in the eroded volume from the Richards equation was 0.02 $m^3\ m^{-1}15\ min^{-1}$, and the root-mean-square error (RMSE) was 0.04 $m^3\ m^{-1}15\ min^{-1}$. The peaks in erosion at hours 10.25, 12, and 12.75 were underestimated, while erosion after hour 14 was overestimated.

[61] Next, rather than assume that the dune was always unstable, it was allowed to erode only when the magnitude of F_D exceeded F_S. The ratio of F_S to F_D is shown in Figure 9 (bottom). Setting the modeled erosion rate to 0 $m^3\ m^{-1}15\ min^{-1}$ when the dune was stable yields an estimate of dune erosion including slope stability (Figure 9, middle). This model explained 72% of the observed variance in the observed eroded volume, an improvement over the assumption of a constantly unstable dune. Including slope stability, the model predicted little erosion after hour 14.75, better matching observations, rather than overpredicting erosion as in the previous case. Including a slope stability estimate decreased bias to $-0.01\ m^3\ m^{-1}15\ min^{-1}$, while the RMSE remained the same at 0.04 $m^3\ m^{-1}15\ min^{-1}$. However, the dune was predicted to be stable for hours 8.5–9, while dune slumps were observed during this period.

4.3. Simplified Infiltration Model

[62] In an effort to produce the most simple dune erosion model possible, we explored the Green-Ampt equation, equation (8), as an alternative to the numerical solution of the Richards equation. The most significant difference between these two equations is that equation (8) neglects the continuing infiltration of water through the dune when water is not in contact with the dune face. To determine the effect of neglecting infiltration when the dune is not exposed to swash, we solved the Richards equation using three different time-dependent boundary conditions for the period between hours 10 and 10.25 and compared the results with the distance of infiltration determined using the Green-Ampt equation. The distance of infiltration was quantified as the minimum distance into the dune where moisture content remained at θ_r. The results of this test are plotted in Figure 10.

[63] The depth of infiltration was determined using the Richards equation and known swash elevation time series (Figure 10, first bar, on left-hand side) as the control. The model results for the different equations and boundary conditions were compared with the control.

[64] Infiltration was modeled using the Richards equation and a boundary condition in which the dune was exposed to water continuously for the same period as in known conditions; the model continued to run while the water level was dropped below the dune base for the remainder of the 15 min period modeled to allow continued infiltration of water within the dune (Figure 10, second bar). Using this

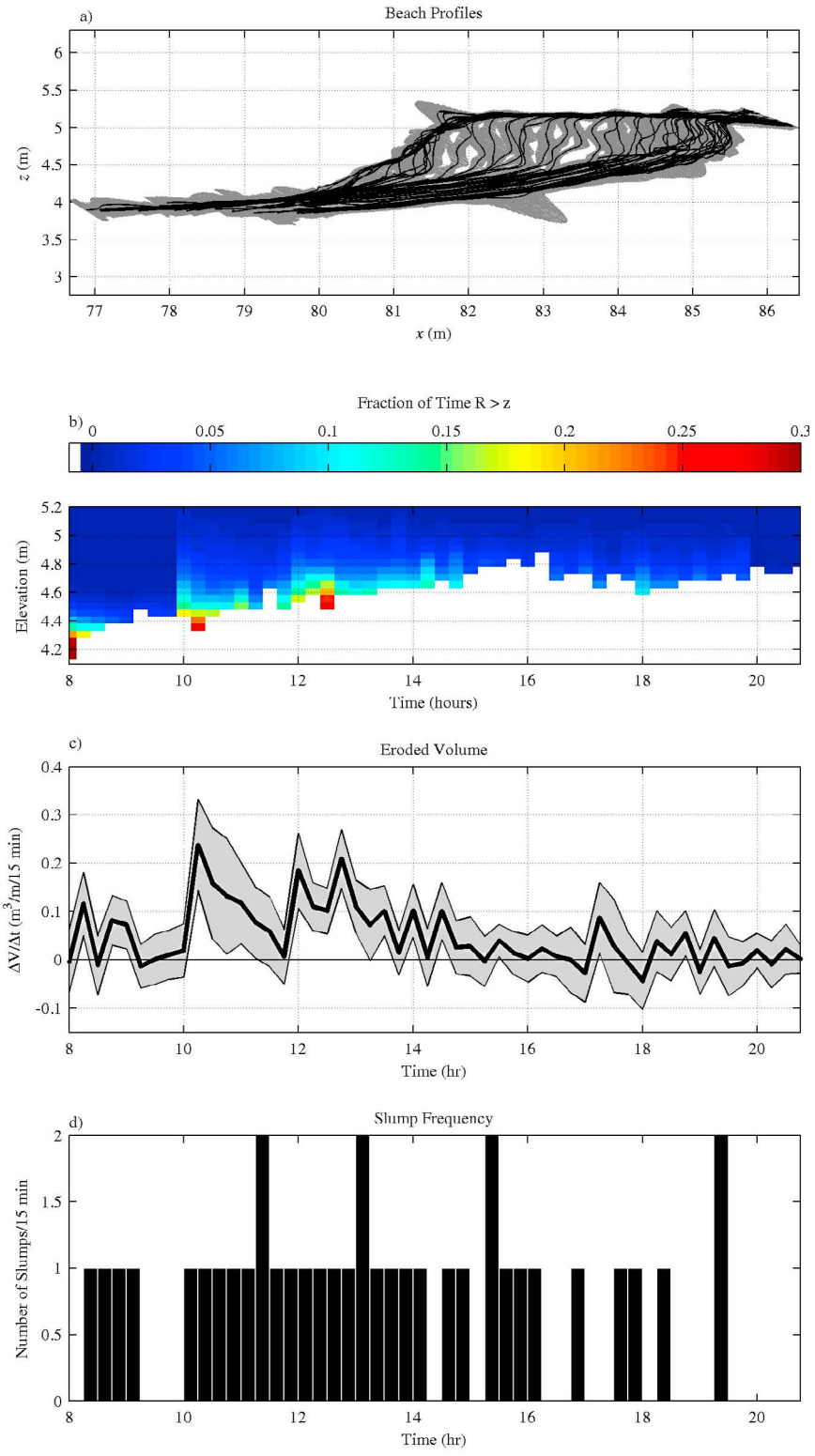

Figure 8. (a) Beach profiles with 95% confidence interval derived from stereo observations. (b) Duration that each elevation on the dune was exposed to swash based on video observations of the swash edge. The white region represents regions of the beach below the dune base. (c) Observations of sediment flux from the dune with 95% confidence interval. (d) Slump frequency for 15 min intervals throughout the experiment.

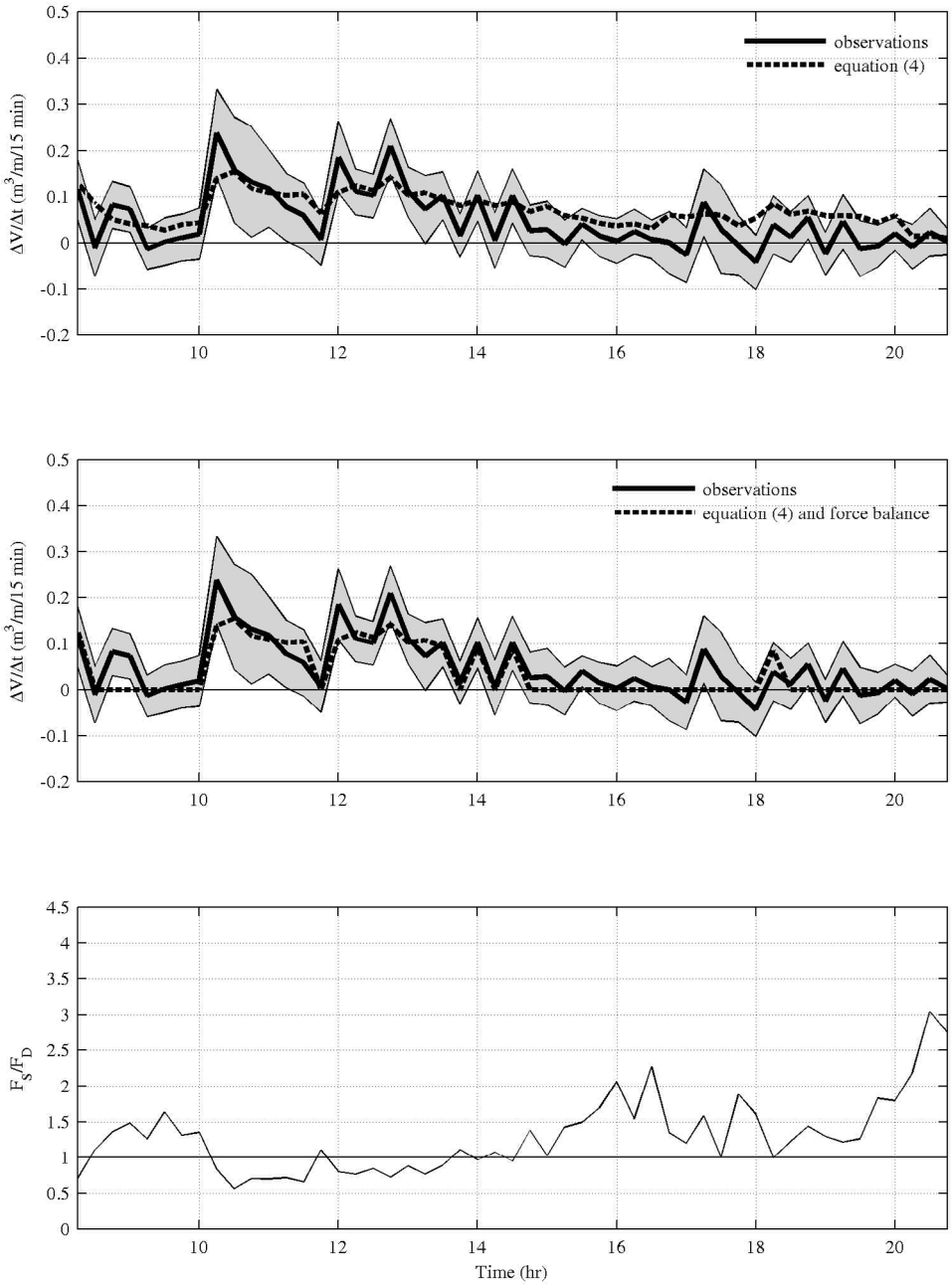

Figure 9. Volume of sediment infiltrated using the Richards equation, equation (4), and (top) known boundary conditions compared with observed erosion, including (middle) slope stability. (bottom) Ratio of F_S to F_D throughout the experiment.

boundary condition, the infiltration was 94% of that modeled with the known swash time series. This result demonstrates that the actual swash time series is not required for reproducing most of the infiltration into the dune.

[65] Then, infiltration was modeled using a boundary condition in which the dune was exposed to water continuously for the same period as in known conditions; then the simulation was stopped (Figure 10, third bar), so that infiltration when water was not in contact with the dune did not occur. Assuming continuous exposure, but not including the extra time for infiltration of moisture when the swash was not in contact with the dune produced an infiltration distance that was 56% of the infiltration distance modeled with the known time series (Figure 10, third bar). Therefore, infiltration when water is not in contact with the dune is an important component of the total infiltration of water into the dune.

[66] Two simpler approaches were also tested. First, infiltration was determined using a boundary condition where the dune was exposed for the same period as in known conditions and infiltration was determined with the Green-Ampt equation assuming the wetted region of the dune was saturated

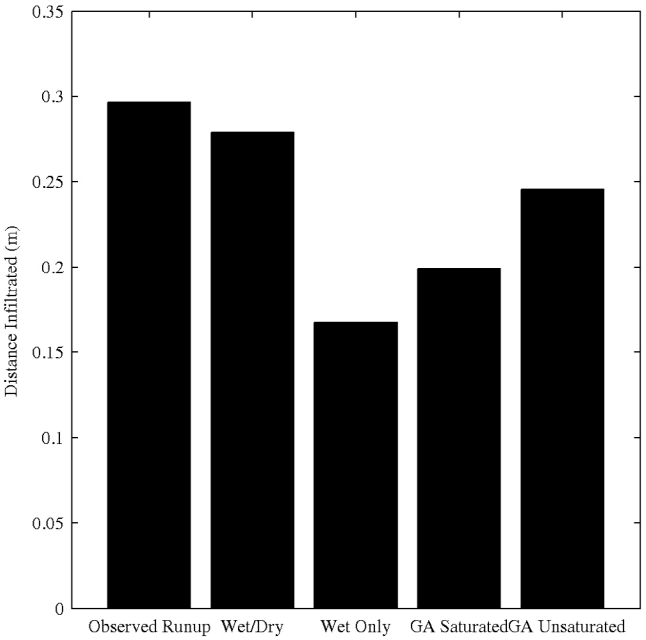

Figure 10. Depth of infiltration determined using the Richards equation and known runup conditions (first bar). Depth of infiltration using a boundary condition in which the dune is exposed to water continuously for the same period as in known conditions; then the water level is dropped for the remainder of the 15 min period (second bar). Depth of infiltration when the dune is exposed to water continuously for the same period as in known conditions; then the simulation is stopped (third bar). Depth of infiltration when the dune is exposed for the same period as in known conditions; infiltration is solved for with the Green-Ampt equation, assuming 100% saturation (fourth bar). Depth of infiltration when the dune is exposed for the same period as in known conditions; infiltration is solved for with the Green-Ampt equation, assuming 70% saturation (fifth bar).

(Figure 10, fourth bar). With this approach, the infiltration distance was 67% of that modeled with the Richards equation and the known time series (Figure 10, fourth bar). The Green-Ampt equation, which does not include the effect of swash intermittency, resulted in an infiltration distance that was within 11% of the Richards equation solution when infiltration of water into the dune during noncontact times was excluded.

[67] Second, infiltration was determined with the same boundary condition and Green-Ampt equation. However, the volumetric water content of wetted region was assumed to be 70% of the saturated value, consistent with the average water content of the wetted portion of the dune at the last time step of the Richards equation solutions for infiltration. Under this assumption the equation produced an infiltration distance that was 83% of the infiltration distance modeled using the Richards equation and the known time series (Figure 10, fifth bar). This suggests that neglecting swash intermittency can be partly compensated for by decreasing the water content from full saturation to 70% saturation for the given sediment properties.

[68] Based on the ratio between infiltration distance from the Green-Ampt equation with 70% saturation and the infiltration from the Richards equation, the coefficient, Λ, in equation (9) was set to 1.2. The combination of setting the saturation to 70% and applying the coefficient, Λ, accounts for the intermittency of swash.

[69] The modified version of the Green-Ampt equation, equation (9), with the assumption that the dune was always unstable, was compared with observations of eroded volume (Figure 11, top). The simplified version of the infiltration model produced error statistics nearly identical to those of the full infiltration model. The modified Green-Ampt equation reproduced 66% of the observed variance in erosion, approximately the same results as the Richards equation. Bias in eroded volume from the modified Green-Ampt equation was 0.00 m^3 m^{-1} 15 min^{-1} and the RMSE was 0.04 m^3 m^{-1}15 min^{-1}. As in the full model, peaks in erosion at hours 10.25, 12, and 12.75 were underestimated and erosion was overpredicted after hour 14.

[70] Next, the slope stability model was included with the simplified model (Figure 11, middle). In this case, the erosion model reproduced 71% of the observed variance, a similar improvement as was found with the full model. The bias in the eroded volume from the combined simplified slope stability model was −0.02 m^3 m^{-1} 15 min^{-1} and the RMSE was 0.04 m^3 m^{-1} 15 min^{-1}. After hour 14.75, F_D exceeded F_S (Figure 11, bottom) and the modeled dune no longer eroded.

4.4. Offshore Wave Forcing

[71] Now that the ability of the Richards equation and slope instability to capture the physics of dune erosion has been demonstrated and the simplification to the infiltration model has been made, the effect of using offshore wave forcing to predict exposure of the dune to swash, equation (13), and resulting dune erosion is tested. Wave height and wave period measured at the wave maker were used as offshore forcing. First, the modeled mean water level, equation (10), and standard deviation of swash, equation (11), are compared with observations (Figure 12) to determine the error associated with statistically representing the transformation of waves through the nearshore region for this experiment. The modeled mean water level explained 81% of the observed variance, the model bias was 0.14 m, and the model RMSE was 0.14 m. The modeled standard deviation of swash explained 81% observed variance, the model bias was −0.05 m, and the RMSE was 0.06 m. The overestimation of $\langle\eta\rangle$ and underestimation of σ produce a distribution that is shifted slightly higher and narrower than the observed distribution of swash, but the modeled distribution is still reasonably representative of the observed distribution.

[72] Next, erosion was determined using infiltration from the modified Green-Ampt equation, offshore wave forcing, and the assumption of an unstable dune to test the effect of parameterized forcing (Figure 13). This model formulation explained 38% of the observed variance, a decrease from known forcing. The bias was 0.03 m^3 m^{-1}15 min^{-1}, and the RMSE was 0.06 m^3 m^{-1}15 min^{-1}. Peaks in erosion at hours 10.25 and 12 were underestimated, and the eroded volume was nearly always overestimated after hour 13. Including the slope stability component of the model improved the explanation of observed variance to 58%. The bias was

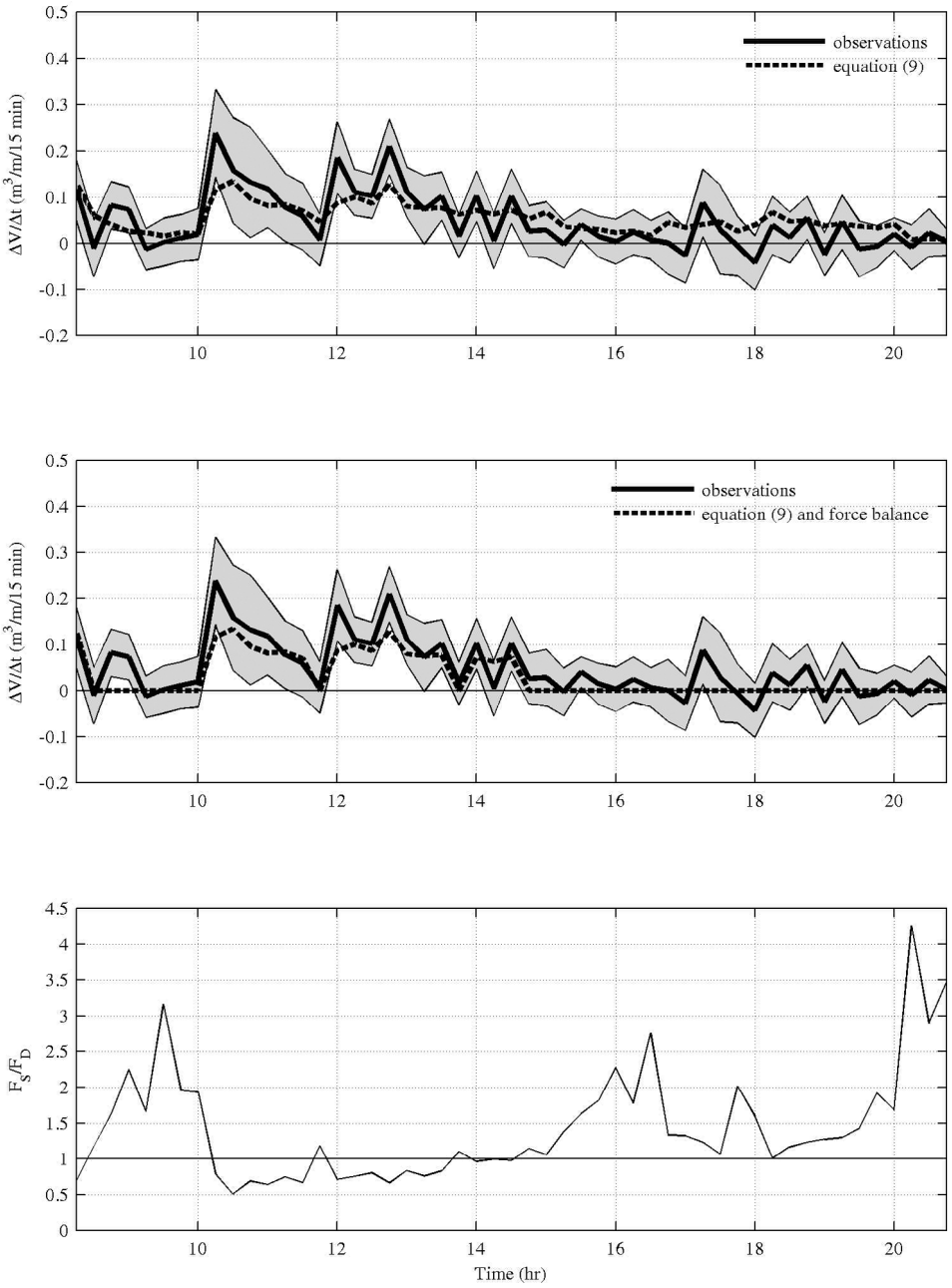

Figure 11. Volume of sediment infiltrated using (top) the calibrated Green-Ampt equation, equation (9), and known boundary conditions compared with observed erosion, including (middle) slope stability. (bottom) Ratio of F_S to F_D throughout the experiment.

reduced to 0.00 m^3 $m^{-1}15$ min^{-1}, and the RMSE was reduced to 0.05 m^3 m^{-1} 15 min^{-1}.

5. Discussion

[73] The dune erosion model developed here is based on the idea that the infiltration of water into the dune and slope stability are the driving mechanisms for dune slumping. The comparison between observations and the full model suggests that these processes contribute significantly to the slumping (R^2 = 0.72), and we have captured the bulk of the processes causing dune erosion in this experiment. It is informative to consider two periods during the experiment when the model underpredicted the observed erosion to understand which processes might control the observed variance in erosion that are not explained.

[74] Slumps occurred between hours 8.5 and 9 that are not explained by the stability model, and, in fact, the ratio of F_S to F_D suggests that the dune should be quite stable. The physical processes controlling dune erosion may have been different during this period than at other times during the experiment. Based on video observations, the dune undercut during this time. When the dune slumped, the failing block overturned and did not erode back to dry sediment, as it did

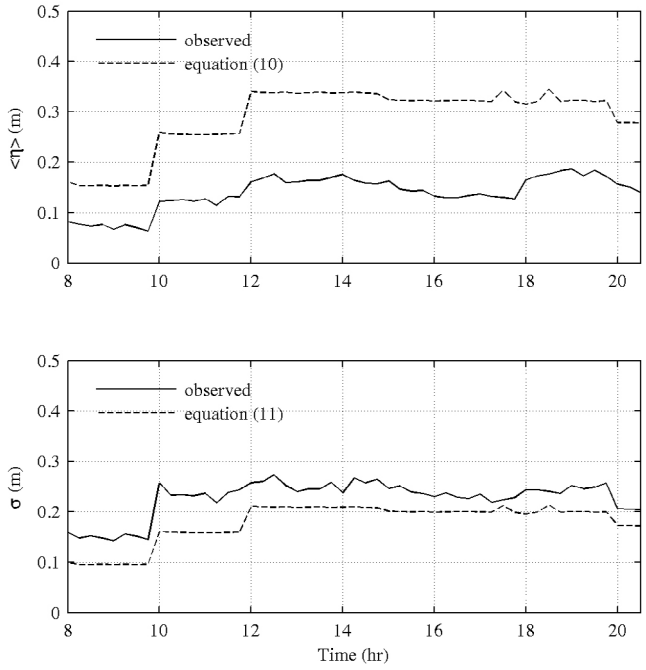

Figure 12. Mean and standard deviation of swash of swash from (top) equation (10) and (bottom) equation (11) plotted with observations.

in the rest of the experiment. An overturning moment that was due to undercutting may have caused the dune to slump between hours 8.5 and 9. In order to capture these slumps, a mechanism for undercutting and elastic beam theory [*Erikson et al.*, 2007] could be included.

[75] The model underpredicted the eroded volume at hours 10.25, 12, and 12.75. At these times, the images show that a significant amount of dry sediment fell after the wetted portion of the dune gave way. Slumping of dry sediment continued until the next swash covered the dune, increasing shear strength of the sediment because of an increase in the apparent cohesion. Ideally, once the initial slump of wet sediment occurred, slope stability of the remaining dry sediment could be determined. Using the model developed here, this is difficult for two reasons. First, after the wet sediment slumps, the elevation of the dune base increases because of the slumped material in front of the scarp. Our model assumes the dune is composed of a vertical scarp, and does not account for this change in morphology or the decrease in scarp height, Δz_0, and increase in stability cause by the position of the slumped material in front of the scarp. Second, we do not resolve slope stability on a wave time scale, so the sequence of wet slump, dry slump, and then runup of the wave to increase shear strength of the dry sediment is not explicitly modeled.

[76] In order to develop this simple model, several assumptions were made for both the infiltration model and the slope stability model. The following paragraphs describe those assumptions.

[77] We chose to model the two-dimensional infiltration of water into the dune face as a series of vertically stacked, decoupled one-dimensional slabs experiencing a vertically variable duration of exposure to runup. This choice allows the use of the simplified Green-Ampt equation, but assumes that the downward percolation of water in the dune is of less importance than the pressure gradient (matrix suction) driving water into the dune. In fact, model results demonstrate that the pore pressure gradient is typically $O(600)$ times larger than the effect of gravity. This choice may affect the vertical distribution of water in the dune, but would not have a large effect on the total amount of water entering the dune. Adopting a multidimensional model, at the expense of simplification, would allow the effect of percolation to be addressed and could be the subject of further work.

[78] The solutions to the infiltration model required the choice of a PTF to relate observed soil characteristics to required hydraulic properties. The chosen PTF [*Schaap and Leij*, 2000] was selected as the most representative of the dune sand used in this experiment. However, other PTFs have been published [*Rawls and Brakensiek*, 1985; *Vereecken et al.*, 1990] based on generally different soil types and the presence of vegetation. Other PTFs would have yielded different hydraulic properties and hence predicted erosion rates. Similarly, even the selected PTF will be sensitive to errors or variability in soil properties. For example, in the practical application of a dune erosion model over a large area, just before a storm, the grain size distribution needed as input to the PTF may not be known. To get an initial feel for the sensitivity to errors in sediment characterization, we investigated the variations in infiltration with example variations in sediment properties.

[79] Given the sediment characteristics of dune sand (95.5% sand, 2.51% silt, and 1.99% clay in this study), we found the *Schaap and Leij* [2000] PTF to be sensitive to the fraction of sand in the grain size distribution. To demonstrate this sensitivity we calculated infiltration distance between hours 10 and 10.25 in the experiment using six different grain size distributions in addition to the observed distribution. The model predicts a 42% decrease in infiltration distance if the sand fraction is decreased from 100% to 95% and a 43% decrease in infiltration when the sand fraction is decreased from 95% to 90%. The model is less sensitive to variation in the small fraction of silt and clay expected in dune sand. Assuming a grain size distribution with 95% sand, 5% silt, and 0% clay produced infiltration distances within 8% of the infiltration produced by a grain size distribution with 95% sand, 2.5% silt, and 2.5% clay. The range of sand fraction in the two replicated measurements for our dune sands was 0.08%, suggesting that the deviation in measured grain size distribution should contribute relatively little to model error.

[80] The PTF is also sensitive to bulk density of the sediment. We calculated infiltration for hours 10–10.25 using three different bulk densities, in addition to the observed bulk density. The infiltration model predicts a 29% decrease in infiltration distance when bulk density is increased from 1.59 to 1.86 g/cm^3 and a 9% decrease in infiltration distance when bulk density is increased from 1.86 to 1.99 g/cm^3.

[81] We assumed the initial condition of the dune was nearly dry for each 15 min simulation. However, in the experiment, waves were run in 15 min increments, and then waves were stopped for at least 45 min (and potentially overnight or over a weekend) to allow low-frequency energy in the tank to subside before the experiment was

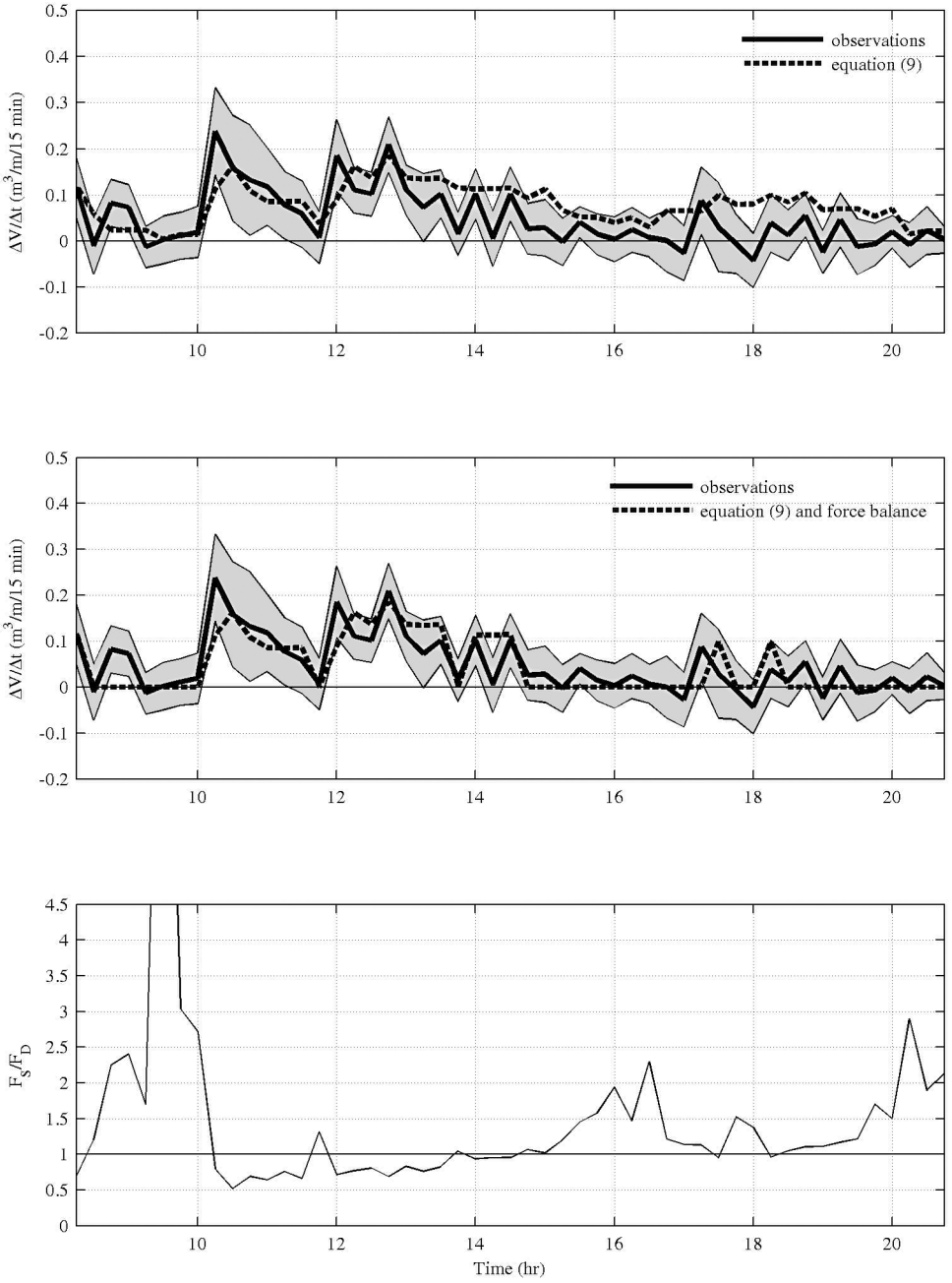

Figure 13. Volume of sediment infiltrated using (top) the modified Green-Ampt equation, equation (9), and boundary conditions from equation (13) compared with observed erosion, including (middle) slope stability. (bottom) Ratio of F_S to F_D throughout the experiment.

continued. During the interim between waves impacting the dune, water would have continued to infiltrate. Because of the presence of water from previous runs, the dune may have been heavier but may also be stronger because of the higher apparent cohesion of partially saturated sediment.

[82] An additional assumption was needed to model infiltration based on the Green-Ampt equation, the coefficient to account for the intermittency of swash, Λ. Based on the comparison with the solution of the Richards equation, $\Lambda = 1.2$. While accurate for our experiment, this coefficient may not be universally applicable; it depends on both the height of swash above the dune base and on the frequency of swash. Therefore it is recommended that the dependence of Λ on the characteristics of swash be tested further.

[83] An alternative approach to applying a coefficient to account for swash intermittency is to tune the infiltration distance calculated with the Green-Ampt equation using the change in volumetric water content, $\Delta\theta$, in equation (8) to match results from the solution to the Richards equation. The eroded volume calculated using this approach was similar to results obtained using Λ ($R^2 = 0.66$, bias = 0.00 $m^3\ m^{-1}15\ min^{-1}$, RMSE = 0.04 $m^3\ m^{-1}15\ min^{-1}$).

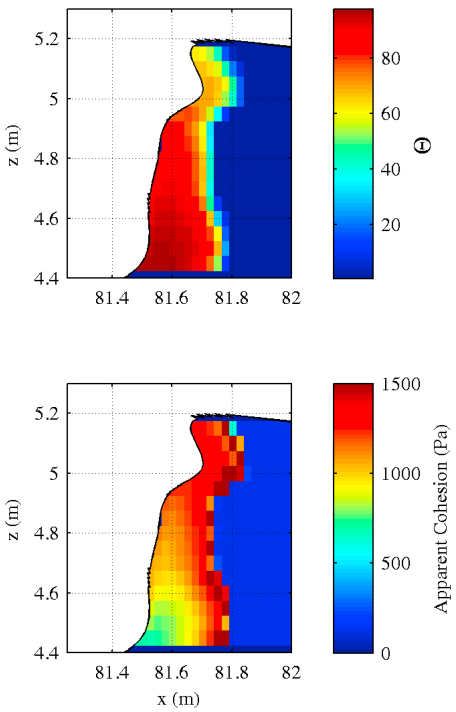

Figure 14. Modeled infiltration into the dune suggests that the moisture content was not homogeneous.

[84] This dune erosion experiment was designed to test existing theories for dune erosion. Because no previous theory included infiltration as a controlling factor on dune stability, water content, pore water pressure, and infiltration were not measured directly. We dealt with the lack of infiltration observations by assuming infiltration was related to erosion. Further experimentation is needed to verify this assumption.

[85] The second component of the dune erosion model, slope stability, also required several assumptions. First, it was assumed that the dune scarp was vertical prior to slumping. This suggests that swash zone processes removed all of the slumped sediment from the front of the dune, although they were not explicitly modeled. This assumption was based on the observation that slumped material at the dune base was always eroded before the next slump occurred. Including the dune erosion model described here within a swash zone sediment transport model would remove the need for this assumption and allow the full relationship between dune slumping and foreshore dynamics to be modeled, but would significantly complicate the calculations.

[86] Because we applied a relatively simple force balance for slope stability, we assumed that the dune was composed of a wet region and a dry region, each with different, homogeneous values of water content and pore water pressure and a vertical contact between the wet and dry regions. However, infiltration model results demonstrate that water was not evenly dispersed throughout the wet portion of the dune (Figure 14). In fact, infiltration can be sufficient to reach near-saturation conditions at the base of the dune, leading to a loss of cohesive strength and to potential dune collapse.

[87] The vertical variation of infiltration that is due to vertical variations in the exposure to runup also introduces a small complication in the model. If only the wetted portion of the dune sediments slumps, an overhang of dry dune sediments would be left after each slump. With low cohesive strength, this overhang would typically also fail and contribute to the eroded volume. Thus, for cases of strong vertical variations in wetting, the eroded volume that would be predicted strictly because of infiltration would be an underestimate. The good agreement of model and data for this experiment presumably implies that this was not a common situation.

[88] Similarly, we have assumed a constant value for porosity throughout the dune. *Nishi et al.* [1999] observed a vertical variation in the compaction of the dune. Given the sensitivity of the infiltration model to porosity and the dependence of slope stability on porosity (equation (25)), variability in compaction may play a role in governing the depth of infiltration and slope stability. Lower porosity at the base of the dune may decrease infiltration distance and at the same time increase shear strength, while higher porosity near the top of the dune would have the inverse effect. Adopting vertically varying porosity and a more complex slope stability model, for example [*Morgenstern and Price*, 1965], which relaxes the trapezoidal slumping block assumption, would allow the stability of a dune with heterogeneous pore water content and porosity to be determined.

[89] Several factors may affect dune erosion under natural conditions that are not addressed in this laboratory experiment. First, the experiment was conducted in an indoor wave flume with an unvegetated dune constructed with earth-moving equipment. A natural dune would likely be produced by aeolian transport (although many dunes are rebuilt by bulldozers after storms) and may be covered with vegetation. The method of dune construction would affect porosity and thus the rate of infiltration and slope stability. Likewise, vegetation affects both infiltration and slope stability. In a natural setting, dune erosion would likely be accompanied by rain, affecting the initial conditions for the infiltration model and slope stability.

[90] Although the laboratory experiment did not include these factors, the infiltration model could account for differences in porosity by changing the sediment characteristics when solving for hydraulic properties with the PTF. The effect of vegetation may also be included in the infiltration and slope stability models. A significant body of literature for including the effects of vegetation on soils exists.

[91] In our experiment, the magnitude of the pressure gradient that is due to matric suction controlled infiltration. In field conditions, the pressure of swash impacting the dune may be larger than in the wave flume. This effect could easily be modeled by increasing the pressure acting on the dune face in the infiltration model boundary condition.

[92] Despite the simplifications made in this model, the two basic processes of infiltration and slope stability capture the majority of observed variance in erosion rate. The model could be further extended in two ways. First, we chose to model slope stability at discrete times, every 15 min throughout the experiment. By coupling the slope stability and infiltration model, the timing of slumps may be modeled by determining slope stability at higher resolution. Second, we found that the eroded volume could be modeled with significant accuracy knowing only cumulative wetting time and not the actual time series of swash edge elevation. Here

we coupled the slope stability model with a simple parameterization for the vertical distribution of swash. The model may also be coupled with a more complex phase-resolving model for swash to force infiltration.

6. Conclusions

[93] We developed a simple model for dune erosion by slumping based on two concepts. The first is that water from swash horizontally infiltrates the dune, increasing the total weight of the dune and promoting its instability and collapse. Infiltration was modeled using a numerical solution to Darcy's law for flow through porous media substituted into the continuity equation and known forcing conditions. The second important concept is the role of slope stability in determining whether the excess overburden of infiltrated water will cause a slump. This was modeled in terms of the balance of destabilizing and stabilizing forces associated with the overburden and yields stability determinations as a function of weight of the wetted sediment and lateral earth force. Because the infiltration of swash increases the apparent cohesion of a dry dune and strength of the wetted volume, it was assumed that the wetted sediments fail as an intact block and that the eroded volume can be equated to the calculated wetted volume, simplifying the dune erosion prediction. Finally, the slumped volume was assumed to be transported offshore by swash zone processes.

[94] The model was tested in a large-scale laboratory dune erosion experiment using time-dependent wave forcing. Error statistics (R^2 = 0.72, bias = −0.01 m^3 $m^{-1}15$ min^{-1}, and RMSE = 0.04 m^3 $m^{-1}15$ min^{-1}) suggest that we capture the majority of the physics controlling dune erosion in this experiment.

[95] In order to produce a model for practical application to dune forecasting, two levels of simplifications were explored. The first simplification replaced the numerical solution for infiltration with *Green and Ampt*'s [1911] equation for infiltration. Error statistics for the simplified model were similar to the solution of the Richards equation (R^2 = 0.71, bias = −0.02 m^3 $m^{-1}15$ min^{-1}, and RMSE = 0.04 m^3 $m^{-1}15$ min^{-1}), suggesting the simplified model can be applied with as much confidence as the full model.

[96] Finally, the simplified model was tested using forcing from a parameterized distribution for swash elevation given only offshore wave conditions [*Stockdon et al.*, 2006]. The parameterized model reproduced the mean and standard deviation of observed swash well (R^2 = 0.81 for both the mean and the standard deviation of swash). The increase in error for this simplified model (R^2 = 0.58, bias = 0.00 m^3 $m^{-1}15$ min^{-1}, and RMSE = 0.05 m^3 $m^{-1}15$ min^{-1}) was caused by use of the parameterized distribution of swash. Still, the simplified model with parameterized forcing explains enough variance to potentially be useful for short- and long-term predictions of dune erosion.

[97] **Acknowledgments.** This work was funded under the Office of Naval Research Coastal Geosciences grants N00014-07-1-0490 and N00014-09-1-0121 and ONR SECNAV/CNO Chair program, N00014-03-1-0973. The authors would like to thank John Stanley for his tireless work with the Argus camera system, the staff of the Hinsdale Wave Research Laboratory, especially Tim Maddux, for experimental design and collection of in situ data. The authors are also grateful to H. Tuba Özkan-Haller and Peter Ruggiero for their comments and suggestions along the way and to Huck Brodersen for encouragement during the writing process.

References

Erikson, L. H., M. Larson, and H. Hanson (2007), Laboratory investigation of beach scarp and dune recession due to notching and subsequent failure, *Mar. Geol.*, *245*(1–4), 1–19, doi:10.1016/j.margeo.2007.04.006.

Fisher, J. S., M. F. Overton, and T. Chisholm (1986), Field measurements of dune erosion, paper presented at the 20th International Conference on Coastal Engineering, Am. Soc. Civ. Eng., Taipei, Taiwan.

Green, W. H., and G. A. Ampt (1911), Studies on soil physics, part I: The flow of air and water through soils, *J. Agric. Sci.*, *4*(1), 1–24.

Holman, R. A., and J. Stanley (2007), The history and technical capabilities of Argus, *Coastal Eng.*, *54*(6–7), 477–491, doi:10.1016/j.coastaleng.2007.01.003.

Hornbaker, D. J., R. Albert, I. Albert, A. L. Barabasi, and P. Schiffer (1997), What keeps sandcastles standing?, *Nature*, *387*(6635), 765, doi:10.1038/42831.

Kriebel, D. L., and R. G. Dean (1985), Numerical simulation of time-dependent beach and dune erosion, *Coastal Eng.*, *9*(3), 221–245, doi:10.1016/0378-3839(85)90009-2.

Larson, M., and N. C. Kraus (1989), SBEACH: Numerical model for simulating storm induced beach change, report, U.S. Army Corps Eng. Coastal Eng. Res. Cent., Vicksburg, Miss.

Larson, M., L. Erikson, and H. Hanson (2004), An analytical model to predict dune erosion due to wave impact, *Coastal Eng.*, *51*(8–9), 675–696, doi:10.1016/j.coastaleng.2004.07.003.

Lohnes, R. A., and R. L. Handy (1968), Slope angles in friable loess, *J. Geol.*, *76*(3), 247–258, doi:10.1086/627327.

Lu, N., T.-H. Kim, S. Sture, and W. J. Likos (2009), Tensile strength of unsaturated sand, *J. Eng. Mech.*, *135*(12), 1410–1419, doi:10.1061/(ASCE)EM.1943-7889.0000054.

McCarthy, D. (2007), *Essentials of Soil Mechanics and Foundations: Basic Geotechnics*, Prentice Hall, Upper Saddle River, N. J.

Morgenstern, N. R., and V. E. Price (1965), The analysis of the stability of general slip surfaces, *Geotechnique*, *15*(1), 79–93, doi:10.1680/geot.1965.15.1.79.

Nishi, R., N. C. Kraus, M. Sato, and T. Uda (1999), Compaction of beaches and dunes, paper presented at Coastal Sediments 1999, Am. Soc. Civ. Eng., Long Island, N. Y., 21–23 June.

Overton, M. F., and J. S. Fisher (1988), Simulation modeling of dune erosion, paper presented at the International Conference on Coastal Engineering, Am. Soc. Civ. Eng., Costa del Sol-Malaga, Spain, 20–25 June.

Overton, M. F., J. S. Fisher, and K. N. Hwang (1994a), Development of a dune erosion model using SUPERTANK data, paper presented at the Twenty-Fourth International Conference on Coastal Engineering, Am. Soc. Civ. Eng., Kobe, Japan.

Overton, M. F., W. A. Pratikto, J. C. Lu, and J. S. Fisher (1994b), Laboratory investigation of dune erosion as a function of sand grain-size and dune density, *Coastal Eng.*, *23*(1–2), 151–165, doi:10.1016/0378-3839(94)90020-5.

Palmsten, M. L., and R. A. Holman (2011), Laboratory investigation of dune erosion using stereo video, *Coastal Eng.*, in press.

Rawls, W. J., and D. L. Brakensiek (1985), Prediction of soil water properties for hydrologic modeling, paper presented at the Symposium on Watershed Management in the Eighties, Am. Soc. Civ. Eng., New York.

Richards, L. A. (1931), Capillary conduction of liquids through porous media, *Physics*, *1*(5), 318–333, doi:10.1063/1.1745010.

Roelvink, D., A. Reniers, A. van Dongeren, J. van Thiel de Vries, R. McCall, and J. Lescinski (2009), Modelling storm impacts on beaches, dunes and barrier islands, *Coastal Eng.*, *56*(11–12), 1133–1152, doi:10.1016/j.coastaleng.2009.08.006.

Schaap, M. G., and F. J. Leij (2000), Improved prediction of unsaturated hydraulic conductivity with the Mualem-van Genuchten model, *Soil Sci. Soc. Am. J.*, *64*(3), 843–851, doi:10.2136/sssaj2000.643843x.

Šimůnek, J., M. T. v. Genuchten, and M. Šejna (2005), The HYDRUS-1D software package for simulating the movement of water, heat, and multiple solutes in variably saturated media, version 3.0, HYDRUS Software Series 1, report, Dept. Environ. Sci., Univ. of Calif. Riverside.

Stockdon, H. F., R. A. Holman, P. A. Howd, and A. H. Sallenger (2006), Empirical parameterization of setup, swash, and runup, *Coastal Eng.*, *53*(7), 573–588, doi:10.1016/j.coastaleng.2005.12.005.

Terzaghi, K., and R. Peck (1967), *Soil Mechanics in Engineering Practice*, 729 pp., John Wiley, New York.

van Genuchten, R. (1980), A losed-form equation for predicting the hydraulic conductivity of unsaturated soils, *Soil Sci. Soc. Am. J.*, *44*(5), 892–898, doi:10.2136/sssaj1980.03615995004400050002x.

van Rijn, L. C. (2009), Prediction of dune erosion due to storms, *Coastal Eng.*, *56*(4), 441–457, doi:10.1016/j.coastaleng.2008.10.006.

Vanapalli, S. K., D. G. Fredlund, D. E. Pufahl, and A. W. Clifton (1996), Model for the prediction of shear strength with respect to soil suction, *Can. Geotech. J.*, *33*(3), 379–392, doi:10.1139/t96-060.

Vereecken, H., J. Maes, and J. Feyen (1990), Estimating unsaturated hydraulic conductivity from easily measured soil properties, *Soil Sci.*, *149*(1), 1–12, doi:10.1097/00010694-199001000-00001.

Wösten, J. H. M., Y. A. Pachepsky, and W. J. Rawls (2001), Pedotransfer functions: Bridging the gap between available basic soil data and missing soil hydraulic characteristics, *J. Hydrol. Amsterdam*, *251*(3–4), 123–150, doi:10.1016/S0022-1694(01)00464-4.

R. A. Holman, College of Oceanic and Atmospheric Sciences, Oregon State University, 104 COAS Administration Bldg., Corvallis, OR 97331, USA.

M. L. Palmsten, Naval Research Laboratory, Code 7430, Stennis Space Center, MS 39529, USA. (margaret.palmsten.ctr@nrlssc.navy.mil)